LANGMUIR

Article

pubs.acs.org/Langmuir

Drag Reduction by Bubble-Covered Surfaces Found in PDMS Microchannel through Depressurization

Yang Gao,[†] Jiang Li,[‡] Ho Cheung Shum,[§] and Haosheng Chen*[,†]

[†]State Key Laboratory of Tribology, Tsinghua University, Beijing 100084, China

[‡]Mechanical engineering school, University of Science and Technology Beijing, Beijing 100083, China

[§]Department of Mechanical Engineering, University of Hong Kong, Pokfulam Road, Hong Kong

Supporting Information

ABSTRACT: Drag reduction was found in polydimethylsiloxane (PDMS) microchannels when the flow was pulled by depressurization at the inlet, and it was attributed to the formation of the bubbles on the PDMS surface. The formed bubbles were examined by atomic force microscopy (AFM), and the resultant effective slip length was measured by microparticle image velocimetry (μPIV). The drag reduction was found to decrease as the bubbles grew and detached from the surface, causing a pulsatile flow in the microchannel.

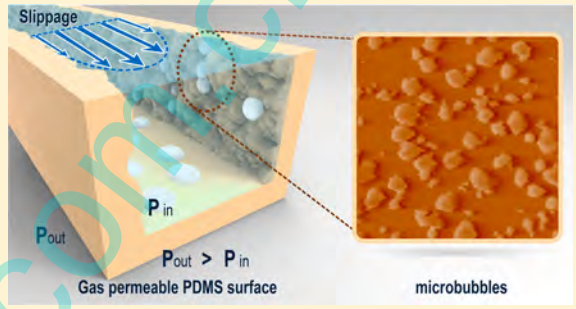

1. INTRODUCTION

The drag reduction property of superhydrophobic surfaces is of growing interest to the transport of liquids on a solid surface.[1] The superhydrophobic surfaces formed in nature[2] or designed artificially[3−6] often have microscopic textures trapping gases, such as air, on its surface separating the flowing fluid from the solid surface. Nanobubbles have been experimentally observed on many kinds of surfaces, such as the silanated silica surface, glass surface,[7,8] and the highly oriented pyrolytic graphite (HOPG) surface.[9] This gaseous layer can provide a heterogeneous slip boundary and reduce the drag experienced by the liquids flowing on it. The extent of drag reduction has been shown to depend on the shape and stability of the bubble.[10] The generation of microbubbles on the solid surface can facilitate drag reduction.[11]

Despite the promise of drag reduction by bubbles, the bubble cushion on the solid surface would be broken when the liquid flowing over it exerted a significant shear,[12] compromising the drag reduction on the superhydrophobic surface. It is therefore necessary to continuously form and reform the bubble-covered surface to sustain the drag reduction effect. Gas infusion,[10] electrolysis,[13] and cavitation[14] have been investigated to generate bubbles on the solid surfaces continuously, but these approaches either necessitate extra gas sources or electrodes, or require an impractically high flow velocity for generating cavitation in microchannels. Alternatively, this bubble-covered surface can be realized through depressurization, where the bubbles will grow under a pressure that is below an atmospheric pressure. Polydimethylsiloxane (PDMS), a widely used material for forming microfluidic devices, is naturally hydrophobic and permeable to gases.[15−17] Air can enter the channel through PDMS and bubbles can grow on its surface, depending on the surrounding pressure in the microchannel.[18] However, this approach to induce bubbles on solid surfaces by depressurization has not been studied, as a way to realize drag reduction up to now.

In this work, the bubbles formed on PDMS under the depressurization condition were examined, and the slip length on this surface in the microchannel was quantitatively measured by microparticle image velocimetry (μPIV). The growth of the bubbles was also found to cause a pulsatile flow and affect the drag reduction. This study reveals the formation of the slip boundary through the bubble growth on a hydrophobic surface in depressurization condition, and it may have potential applications in the drag reduction in microchannels.

2. EXPERIMENTAL SCHEMATICS

The experimental system for investigating the drag reduction consisted of a microfluidic device and a pressure control apparatus, as presented in Figure 1a. Deionized water was driven into the microchannel by the pressure difference between the inlet and outlet, which was controlled by the pressure controller MFCS (Fluigent Co.). The oxygen content of deionized water is 9.3 mg/L, measured by a FireSting oxygen sensor (Pyro Science Co.), corresponding to the gas content of 25.1 mg/L (100% of saturation). The microfluidic device was made of PDMS using soft lithography technology.[19] The channel was first filled with triethoxy(octyl)silane (OTES, Sigma-Aldrich) solution for 15 min at 105 °C to make the surface hydrophobic, and then the channel was washed with deionized water. The contact angles of the treated PDMS and treated glass surfaces are 106° and 84°, respectively. The microchannel has a rectangular shape with a height of h = 40 μm and a width of W = 100 μm, as shown in Figure 1b.

Received: March 28, 2016
Revised: April 27, 2016
Published: April 28, 2016

DOI: 10.1021/acs.langmuir.6b01186
Langmuir 2016, 32, 4815−4819

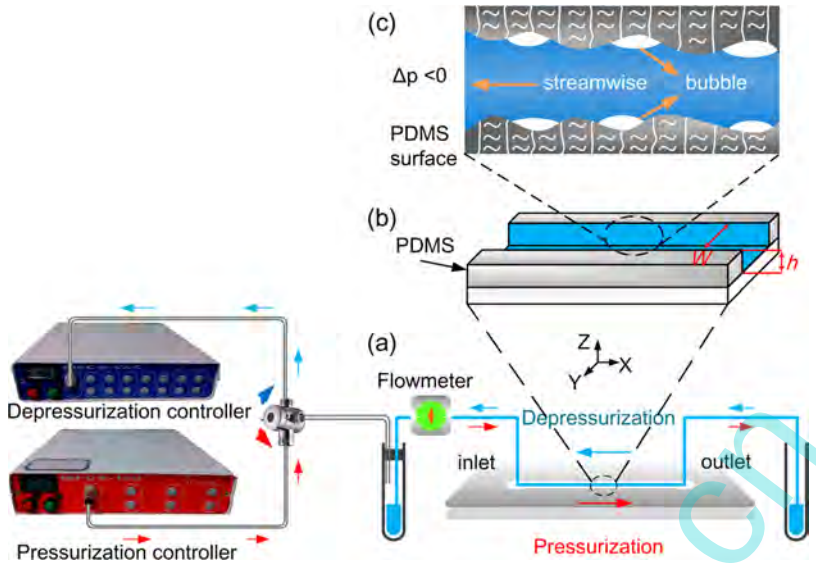

Figure 1. (a) Schematic of flow in microchannels made of hydrophobic permeable materials. The driven pressure in the channel was lower than the atmospheric pressure ($\Delta p < 0$), where bubbles were generated on the surface of the channel wall. (b) Enlarged view of the rectangular shaped microchannel. (c) Schematic of the bubble-covered surface formed under the depressurization conditions.

Using the pressurization-driven method, the pressure was higher than the atmospheric pressure at the inlet, while the outlet was open to the atmosphere. Consequently, water was pushed from the inlet to the outlet, as illustrated by the red arrows in Figure 1a. Using the depressurization-driven method, the water in the microchannel was pulled by the depressurization provided by the depressurization controller, with 0.1% precision. Thus, water was sucked from the outlet to the inlet, as illustrated by the blue arrows in Figure 1a.

Bubbles were expected to form on the PDMS surface by depressurization and cause the slip boundary, as illustrated by Figure 1c. In the pressurization experiments, the driven pressure was controlled from 1000 mbar to 1400 mbar, while in the depressurization experiments, the driven pressure was controlled from 1000 mbar to 600 mbar. The environment pressure is 1000 mbar in both of the experiments. A calibration is done for each measurement to set the zero pressure to environmental pressure. The flow rates of the water in the microchannel were measured by a flowmeter (Fluigent Co. Its measuring range was 0−80 μL/min, and the resolution was 0.06 μL/min, with a precision of 0.5%.), which was connected at the upstream of flow.

3. DRAG REDUCTION FLOW BY DEPRESSURIZATION

Under the same pressure difference ($\Delta p = |p_{inlet} - p_{outlet}|$) the flow rates of water were found to change significantly under the two different driven methods, as shown in Figure 2a. For example, the flow rates in depressurization condition were higher than those in pressurization condition when Δp was lower than 150 mbar. The increased flow rate suggests a drag reduction under the depressurization-driven condition. The drag reduction was expressed by eq 1, where Q_D was the average flow rate in depressurization condition and Q_P was the average flow rate in pressurization condition.

$$DR\% = \frac{Q_D - Q_P}{Q_P} \times 100\% \quad (1)$$

The drag reduction under different driven pressure is presented by the green symbols and the green y axis in Figure 2a. Drag reduction was obvious when $\Delta p < 150$ mbar. It should be noted here that the drag reduction at $\Delta p = 50$ mbar had a relatively large standard deviation, since the flow rates were

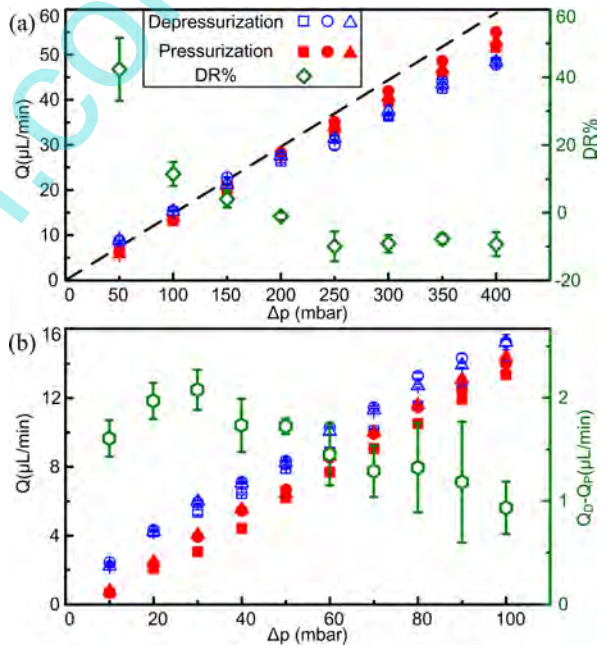

Figure 2. Different symbols indicate the average flow rates measured in three devices with the same channel size. Error bars indicate different flow rates in one device. For each Δp, the average value was obtained from 15 flow rate values. Red and the blue symbols represent fluid under pressurization and depressurization-driven condition, respectively. (a) Green symbols show average drag reduction. Error bars indicate different drag reduction in three devices. Black dashed line represents theoretical flow rate in microchannel (Supporting Information A). (b) Average flow rates from 10 mbar to 100 mbar. Green symbols show average calculated flow rates difference.

relatively low and the small variation of the flow rates would cause a large change in the drag reduction according to eq 1.

It was also found that the drag reduction decreased as Δp increased. When Δp was 200 mbar, drag reduction was too small that can be neglected. As Δp continued to increase, the drag reduction effect disappeared and the drag force even increased. To show the drag reduction more clearly, the details

DOI: 10.1021/acs.langmuir.6b01186
Langmuir 2016, 32, 4815−4819

of the flow rates within the range of 10−100 mbar are presented in Figure 2b. The positive flow rate difference supports the existence of the drag reduction under the depressurization condition.

The change in flow rate was not caused by the change in channel geometry in two different driven methods. Deformations of PDMS channel under pressurization and depressurization condition were measured (Supporting Information B). The deformations were too small to cause such changes in flow rates. Moreover, the channel becomes narrower in depressurization condition, and it would have resulted in a decrease in the flow rate. Thus, the drag reduction could not have been accounted for by the deformation of the channel. Also, to confirm whether the system is symmetric, we measured the flow rates by controlling both inlet and outlet pressures, and confirmed that the system is symmetric (Supporting Information C). Therefore, the drag reduction was attributed to the variation of the PDMS surface under depressurization condition.

4. SLIP BOUNDARY OF PDMS SURFACE

The surface condition of PDMS was examined via atomic force microscopy (AFM; CSPM4000, Benyuan Co.). The whole AFM system was put in a vacuum chamber (Supporting Information D and E), where the inner pressure can be controlled from 1000 mbar to 850 mbar. The PDMS samples were also treated by OTES to render its surface hydrophobic, same as the channel surface used in drag reduction experiments. Profiles of the PDMS surface were measured by tapping mode of AFM. The dry PDMS substrate was measured first (Supporting Information F). The surface was smooth, and no protrusion was observed. Then, PDMS surface was measured in water, and there are some protrusions with average diameters of 3.10 ± 0.92 μm on PDMS surface, as shown in Figure 3a1. The protrusions have a positive shift of phase, indicating the protrusions were softer than the substrate surface,[7,9] as shown in Figure 3a2. As the ambient pressure decreased to 850 mbar, the number and size of these protrusions both increased, as shown in Figure 3b1. The average diameter of the protrusions was 6.54 ± 1.72 μm. Detail statistical analysis of these protrusions is provided in Supporting Information G. These protrusions found on water-covered hydrophobic surfaces were usually considered to be microbubbles on the substrate.[7] In this experiment, the increased number and size of the softer protrusion caused by depressurization also suggests microbubbles growth from nuclei on hydrophobic surface.

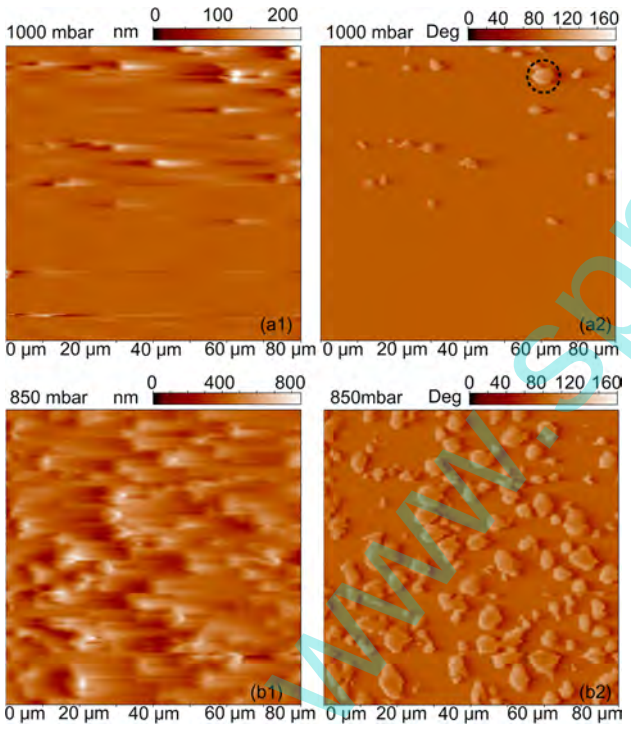

Figure 3. Microbubbles on the PDMS surface scanned by the AFM. (a1) The 80 × 80 μm^2 AFM tapping mode image showing the profile of the bubbles on a PDMS surface in water at the pressure of 1000 mbar. (a2) Corresponding phase image of (a1). The black circle highlights a positive shift of the phase. (b1) Profile of the bubbles on a PDMS surface at the pressure of 850 mbar, and (b2) corresponding phase image. The images were obtained at a scan rate of 1 Hz, 512 × 512 pixel resolution by using a tapping-mode scanning probe (PPP-NCHR, Nanosensors).

The generation of the bubbles on the PDMS surface changed the boundary condition for the flow in the microchannel. The generated gas−liquid interface provided a slip boundary, and the effective slip length of the bubble-covered PDMS surface was measured by μPIV (Dantec Co.). Fluorescent particles with a diameter of 1 μm (Carboxylate-Modified Microspheres, Nile red (535/575) FluoSpheres) were added to the deionized water, as shown in Figure 4a. Image pairs with a delay time of 5 μs between two exposures were recorded using a FlowSense EO 4 M camera with a resolution of 3.15 × 3.15 μm^2. The measured velocity profile at the driven pressure of 1350 mbar is presented in Figure 4b. The average flow velocities across the stream (Y direction) were calculated and are presented in Figure 4c. It should be noted there that the pressures in Figure 4c was the local pressure at the measuring position, which was different from the driven pressure. According to the Poiseuille law, the local pressure was calculated to be 41% of the driven pressure at the outlet (Supporting Information A). In depressurization condition, we use a least-squares linear fitting to get the slip length b according to Navier's slip boundary condition: $b = V/(\partial V/\partial Y)|_{(Y=0)}$.The fitting lines and slip length are shown in Figure 4d. Average slip length for three times at the local pressures of 897 mbar, 877 mbar and 856 mbar were 2.09 ± 0.38 μm, 1.78 ± 0.29 μm and 1.39 ± 0.51 μm, respectively. The decreasing effective slip length with the increasing Δp in depressurization condition was considered to be caused by the increasing protrusion angles of the bubbles.[10] The average velocity profiles for the flow in pressurization-driven condition were also measured (Figure 4e), and no slippage was found on the PDMS surface as presented in Figure 4f. The measured slip length further confirmed the transition from the no-slip boundary to the slip boundary of PDMS surface when the flow inside the microchannel was depressurized. Together with the results from AFM, we confirm that the formation of the bubble-covered surface of PDMS is the main reason for the drag reduction under the depressurization-driven condition.

5. BUBBLE GROWTH AND PULSATILE FLOW

The measured drag reduction also indicates that bubbles formed on the microchannel surface do not always cause the drag reduction. On the contrary, the bubbles with large protrusion angles were known to increase the drag force according to the calculation.[10] In this experiment, the bubbles

DOI: 10.1021/acs.langmuir.6b01186
Langmuir 2016, 32, 4815−4819

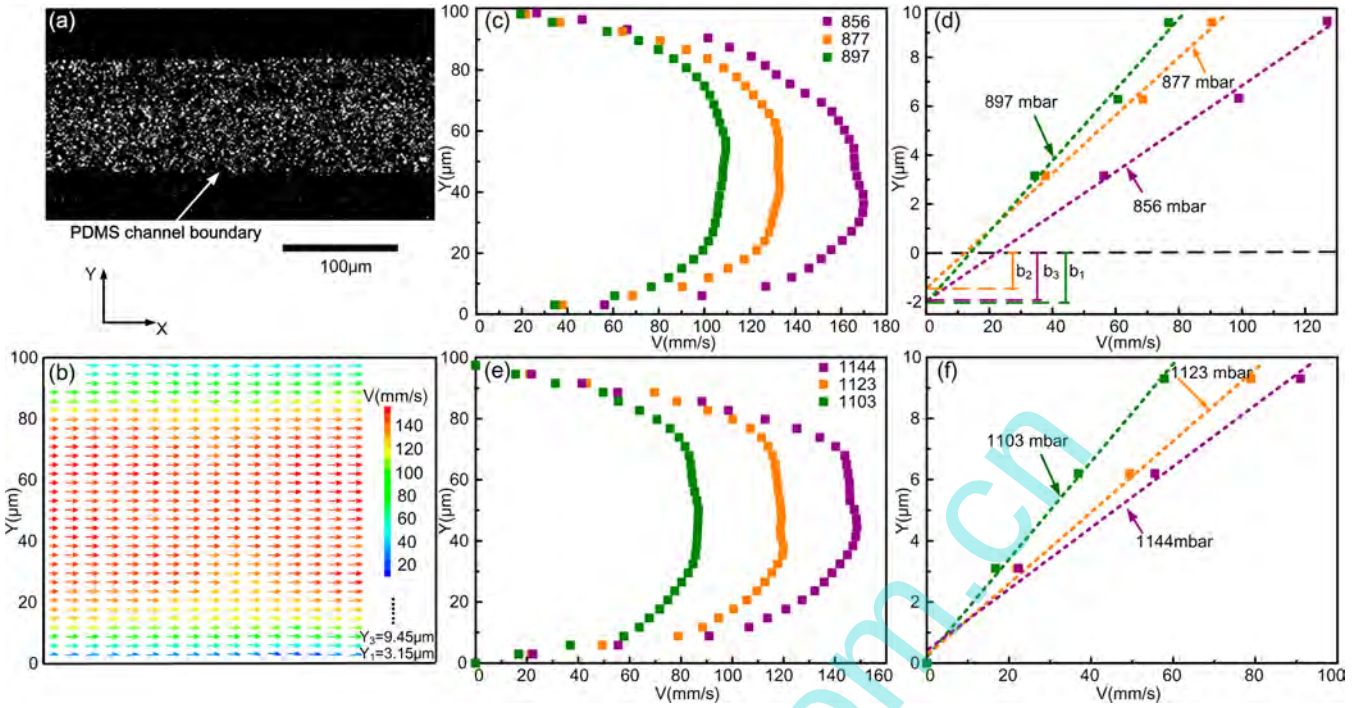

Figure 4. (a) Fluorescence microscope image of the fluorescent particles flowing in the microchannel. (b) μPIV image of velocity field measurement at the driven pressure of 1350 mbar. (c) Average velocity profiles along direction Y, as measured by μPIV at the local pressures of 897, 877, and 856 mbar. (d) Average velocity profiles near PDMS wall surface. Dashed lines represent the linear fits for the b estimation. (e) Average velocity profiles, as measured by μPIV at the pressures of 1103, 1123, and 1144 mbar. (f) Average velocity profiles near PDMS wall under pressurization condition.

on the PDMS surface were observed to grow and finally detached from the surface as the pressure continued to decrease, as shown in Figure 5a1−a3. This growth-to-detachment process of the bubbles caused periodic fluctuation in the depressurization condition, as shown in Figure 5b. The period of the bubble growth λ were measured from the wavelength of the pulsatile flow.

To study the relationship between the bubble growth and the flow rate fluctuation, the flow rates and the images of the bubbles at different stages were recorded simultaneously, as shown in Figure 5a and b. At the early stage of the bubble growth shown in Figure 5a1, the bubble was too small to be observed in microscope and the bubble surface acted as a slip boundary. Therefore, the flow rate reached a maximum value and the drag reduction was increased. However, when the bubble grew larger (Figure 5a2), the bubble protrusion would block the flow and the flow rates decreased. When the bubble reached its largest size and was to detach from the surface (Figure 5a3), the flow rate reached its minimum value. The frequency of the fluctuation became higher when Δp increased in the depressurization condition, as shown in Figure 5c. The increase in frequency with increasing Δp was attributed to the faster growth-to-detachment period of a bubble on the surface. With the increase of the frequency, more bubbles formed and then entered the flow, which would block the flow and increase the drag force. That explains the decrease of the drag reduction when Δp is high than 150 mbar.

It is also important to investigate the influence of gas content of the water in our experiment. The DI water was degassed by a repeated freezing-pumping-melting process.[20] During the melting step, ultrasonic stirring was also used to accelerate the removal of the gas. The whole process was carried out for five times. The degassed water was used immediately after degassing. The measured gas content is 11.6 mg/L, with 46.2% of saturation (Supporting Information H). Using the degassed water, drag reduction has also been found in the depressurization condition. We also varied the gas content to measure bubble growth periods. The value of λ is independent of gas content, as shown in Figure 5d. Although we cannot entirely get rid of the gas from the water, this result supports that the growth of the bubbles on the PDMS surface is mainly through the heterogeneous nucleation under the depressurization condition. Of course, we acknowledge that the growth of the bubble may be affected by many factors, such as the pressure, gas content of water, the surface condition, and so on. In this work, we just reveal the formation of a bubble-covered surface and illustrate its effect on drag reduction in a depressurization condition.

6. CONCLUSIONS

This work presents an approach to achieve drag reduction using a depressurization-driven method to form a bubble-covered surface on the wall of PDMS microchannel. The flow boundary condition at the bubble-covered surface changes from no slip to slip and causes a dramatic drag reduction. Moreover, as the bubbles were growing, the growth-to-detachment process of the bubble induces fluctuation of the flow rate, and decreases the drag reduction. This work helps to understand the origination and evolution of drag reduction on a bubble-covered surface, and the use of depressurization-driven method may have potential applications in drag reduction.

DOI: 10.1021/acs.langmuir.6b01186
Langmuir 2016, 32, 4815−4819

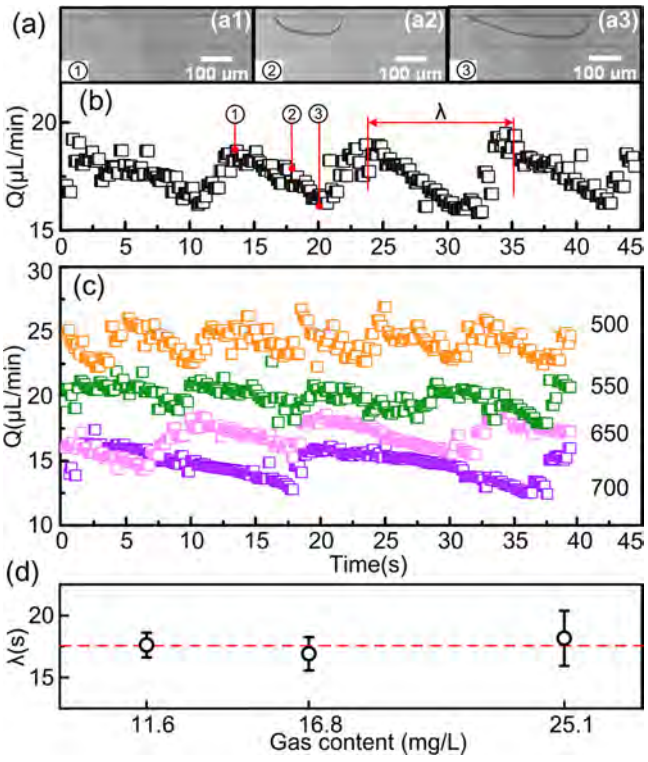

Figure 5. Fluctuation of the flow rate induced by the bubble growth under the depressurization-driven condition. (a) Bottom images of the bubble growth at three different stages observed by an inverted microscope. (b) Plot of the flow rate as a function of time at a pressure of 600 mbar. Flow rates were recorded with the time interval of 0.1s to see the transient flow status caused by the growth of the bubbles. Fluctuation period is denoted λ. (c) Degree of fluctuation in the flow rate increases with the magnitude of the reduced pressure applied. (d) Period of the bubble growth λ versus gas content at the pressure of 600 mbar. Red dashed line shows the average value of λ.

■ ASSOCIATED CONTENT

Supporting Information

The Supporting Information is available free of charge on the ACS Publications website at DOI: 10.1021/acs.langmuir.6b01186.

Calculation of the local pressure and the theoretical flow rate; deformation of the PDMS channel under pressurization and depressurization condition; flow rates measurement by controlling both the inlet and outlet pressures; schematic of the AFM system for characterizing the PDMS surface in water under the depressurization condition; AFM testing experiments; AFM image of dry PDMS substrate; statistical analysis of the protrusion size; gas content and flow rates measurement for DI water and degassed water (PDF)

■ AUTHOR INFORMATION

Corresponding Author

*E-mail: chenhs@tsinghua.edu.cn.

Notes

The authors declare no competing financial interest.

■ ACKNOWLEDGMENTS

This work is supported by the National Natural Science Foundation of China (NSFC) projects (No. 51275266, No. 51322501, and No. 51275036).

■ REFERENCES

(1) Lyu, S.; Nguyen, D. C.; Kim, D.; Hwang, W.; Yoon, B. Experimental drag reduction study of super-hydrophobic surface with dual-scale structures. *Appl. Surf. Sci.* **2013**, *286*, 206−211.
(2) Neinhuis, C.; Barthlott, W. Characterization and distribution of water-repellent, self-cleaning plant surfaces. *Ann. Bot.* **1997**, *79*, 667−677.
(3) Feng, L.; Song, Y.; Zhai, J.; Liu, B.; Xu, J.; Jiang, L.; Zhu, D. Creation of a superhydrophobic surface from an amphiphilic polymer. *Angew. Chem., Int. Ed.* **2003**, *42*, 800−802.
(4) Truesdell, R.; Mammoli, A.; Vorobieff, P.; Van Swol, F.; Brinker, C. J. Drag reduction on a patterned superhydrophobic surface. *Phys. Rev. Lett.* **2006**, *97*, 044504.
(5) Tsai, P.; Peters, A. M.; Pirat, C.; Wessling, M.; Lammertink, R. G.; Lohse, D. Quantifying effective slip length over micropatterned hydrophobic surfaces. *Phys. Fluids* **2009**, *21*, 112002.
(6) Feuillebois, F.; Bazant, M. Z.; Vinogradova, O. I. Effective slip over superhydrophobic surfaces in thin channels. *Phys. Rev. Lett.* **2009**, *102*, 026001.
(7) Ishida, N.; Inoue, T.; Miyahara, M.; Higashitani, K. Nano bubbles on a hydrophobic surface in water observed by tapping-mode atomic force microscopy. *Langmuir* **2000**, *16*, 6377−6380.
(8) Attard, P. Nanobubbles and the hydrophobic attraction. *Adv. Colloid Interface Sci.* **2003**, *104*, 75−91.
(9) Hampton, M. A.; Nguyen, A. V. Nanobubbles and the nanobubble bridging capillary force. *Adv. Colloid Interface Sci.* **2010**, *154*, 30−55.
(10) Karatay, E.; Haase, A. S.; Visser, C. W.; Sun, C.; Lohse, D.; Tsai, P. A.; Lammertink, R. G. Control of slippage with tunable bubble mattresses. *Proc. Natl. Acad. Sci. U. S. A.* **2013**, *110*, 8422−8426.
(11) Lohse, D.; Zhang, X. Surface nanobubbles and nanodroplets. *Rev. Mod. Phys.* **2015**, *87*, 981.
(12) Wexler, J. S.; Jacobi, I.; Stone, H. A. Shear-Driven Failure of Liquid-Infused Surfaces. *Phys. Rev. Lett.* **2015**, *114*, 168301.
(13) Chen, H.; Li, J.; Chen, D. Study of drag forces on a designed surface in bubbly water lubrication using electrolysis. *J. Fluids Eng.* **2006**, *128*, 1383.
(14) Ceccio, S. L. Friction drag reduction of external flows with bubble and gas injection. *Annu. Rev. Fluid Mech.* **2010**, *42*, 183−203.
(15) Wong, I.; Ho, C. M. Surface molecular property modifications for poly (dimethylsiloxane) (PDMS) based microfluidic devices. *Microfluid. Nanofluid.* **2009**, *7*, 291−306.
(16) Mata, A.; Fleischman, A. J.; Roy, S. Characterization of polydimethylsiloxane (PDMS) properties for biomedical micro/nanosystems. *Biomed. Microdevices* **2005**, *7*, 281−293.
(17) Jo, B. H.; Van Lerberghe, L. M.; Motsegood, K. M.; Beebe, D. J. Three-dimensional micro-channel fabrication in polydimethylsiloxane (PDMS) elastomer. *J. Microelectromech. Syst.* **2000**, *9*, 76−81.
(18) Kang, J. H.; Kim, Y. C.; Park, J.-K. Analysis of pressure-driven air bubble elimination in a microfluidic device. *Lab Chip* **2008**, *8*, 176−178.
(19) Xia, Y.; Whitesides, G. M. Soft lithography. *Annu. Rev. Mater. Sci.* **1998**, *28*, 153−184.
(20) Pashley, R. M.; Rzechowicz, M.; Pashley, L. R.; Francis, M. J. De-gassed water is a better cleaning agent. *J. Phys. Chem. B* **2005**, *109*, 1231−1238.

DOI: 10.1021/acs.langmuir.6b01186
Langmuir 2016, 32, 4815−4819